Permeation in the Dihydropyridine-sensitive Calcium Channel

Multi-ion Occupancy but No Anomalous Mole-Fraction Effect between Ba^{2+} and Ca^{2+}

DAVID T. YUE and EDUARDO MARBAN

From the Departments of Medicine and Biomedical Engineering, The Johns Hopkins University School of Medicine, Baltimore, Maryland 21205

ABSTRACT We investigated the mechanism whereby ions cross dihydropyridine-sensitive (L-type) Ca channels in guinea pig ventricular myocytes. At the single-channel level, we found no evidence of an anomalous mole-fraction effect like that reported previously for whole-cell currents in mixtures of Ba and Ca. With the total concentration of Ba + Ca kept constant at 10 (or 110) mM, neither conductance nor absolute unitary current exhibits a paradoxical decrease when Ba and Ca are mixed, thereby weakening the evidence for a multi-ion permeation scheme. We therefore sought independent evidence to support or reject the multi-ion nature of the L-type Ca channel by measuring conductance at various permeant ion concentrations. Contrary to the predictions of models with only one binding site in the permeation pathway, single-channel conductance does not follow Michaelis-Menten kinetics as Ba activity is increased over three orders of magnitude. Two-fold variation in the Debye length of permeant ion solutions has little effect on conductance, making it unlikely that local surface charge effects could account for these results. Instead, the marked deviation from Michaelis-Menten behavior was best explained by supposing that the permeation pathway contains three or more binding sites that can be occupied simultaneously. The presence of three sites helps explain both a continued rise in conductance as $[Ba^{2+}]$ is increased above 110 mM, and the high single-channel conductance (~7 pS) with 1 mM $[Ba^{2+}]$ as the charge carrier; the latter feature enables the L-type channel to carry surprisingly large currents at physiological divalent cation concentrations. Thus, despite the absence of an anomalous mole-fraction effect between Ba and Ca, we suggest that the L-type Ca channel in heart cells supports ion flux by a single-file, multi-ion permeation mechanism.

Address reprint requests to Dr. Eduardo Marban, Hunterian 116, Johns Hopkins University School of Medicine, 725 North Wolfe Street, Baltimore, MD 21205.

J. GEN. PHYSIOL. © The Rockefeller University Press · 0022-1295/90/05/0911/29 $2.00
Volume 95 May 1990 911–939

INTRODUCTION

Dihydropyridine-sensitive, or L-type, Ca channels demonstrate remarkable conduction properties that point to a mechanism whereby ions bind to specific sites in the permeation pathway as they traverse the pore. Under physiologic conditions L-type channels are quite selective for Ca^{2+} and yet support a large flux of Ca^{2+} into the cell. In spite of their high selectivity for divalent over monovalent cations when both are present (Goldman permeability ratios >1,000; Lee and Tsien, 1984), L-type channels can also carry large monovalent currents in the absence of divalent cations (Kostyuk et al., 1983; Almers et al., 1984; Coronado and Affolter, 1986; Hess et al., 1986; Hadley and Hume, 1987). Two general classes of models are capable of explaining these and other distinctive features of ion permeation through L-type Ca channels. The first proposes that divalent cations, when present, bind to a high-affinity site that makes the pore Ca-selective by allosteric modulation. In the absence of Ca^{2+} (or another divalent cation, e.g., Ba^{2+}) the pore loses its selectivity and the channel can support a large flux of monovalent ions (Kostyuk et al., 1983; Kostyuk and Mironov, 1986). The second mechanism envisions a pore studded with two or more sites that bind ions as they traverse the channel. The affinity with which a given ion binds to each site determines selectivity, while high fluxes are maintained as multiple ions occupy the pore simultaneously and propel each other through by electrostatic repulsion. Such single-file, multi-ion permeation models, elaborated earlier for K (Hille and Schwarz, 1978) and Na channels (Begenisich and Cahalan, 1980), have found particular appeal in their application to Ca channels (Hess and Tsien, 1984; Almers and McCleskey, 1984).

A major distinguishing feature that has favored multi-ion occupancy is the "anomalous mole-fraction effect" (AMFE) between Ba^{2+} and Ca^{2+}. This phrase describes the observation that, at a constant concentration of divalent cations, Ca channel current is paradoxically smaller when *mixtures* of Ba^{2+} and Ca^{2+} are presented to the channel, compared with the currents in pure solutions of either. Such a decrease in the current carried by L-type Ca channels has been observed in mixtures of Ba^{2+} and Ca^{2+} in both cardiac (Hess and Tsien, 1984; McDonald et al., 1986; Campbell et al., 1988) and skeletal (Almers and McCleskey, 1984) muscle, as well as in neurons (Byerly et al., 1985). Although gating and premeation are difficult to distinguish in macroscopic currents, the changes in flux seemed clear enough to be interpreted as evidence for multi-ion occupancy. The interaction among permeant divalents has particular significance since, when Ba or Ca ions are present, the simplest allosteric model is reduced to a single-site mechanism inconsistent with an AMFE (Hille and Schwarz, 1978). The paradoxical increase in monovalent current in the absence of divalents represents another manifestation of anomalous mole-fraction behavior (Coronado and Affolter, 1986), but interpretation of these phenomena are complicated because maintenance of normal channel architecture could depend critically on the presence of divalents (Kostyuk et al., 1983; Pietrobon et al., 1988). Thus, the AMFE between divalents constitutes a crucial feature favoring a multi-ion permeation hypothesis.

Unfortunately, the conditions under which anomalous interactions between Ba^{2+} and Ca^{2+} have been observed give reason to wonder whether they reflect genuine permeation properties of the pore. The majority of data have been obtained at the

whole-cell level, where gating and permeation cannot always be dissected unambiguously. Hess and Tsien (1984) used fluctuation analysis to estimate single-channel current (i) and found that i near 0 mV decreased from ~0.07 pA in 10 mM [Ca^{2+}] to ~0.03 pA in 7 mM [Ba^{2+}] + 3 mM [Ca^{2+}] (total [divalent] = 10 mM). Given the fivefold smaller value of their noise-estimated i in 10 mM [Ca^{2+}] as compared with direct measurements of unitary currents (Hess et al., 1986), technical limitations may have biased the estimates of i. Few single-channel recordings have confirmed directly whether such an AMFE is a genuine feature of native L-type Ca channel permeation (Friel and Tsien, 1989), and these apparently conflict with results from skeletal t-tubule Ca channels reconstituted in bilayers that indicate no AMFE between Ba^{2+} and Ca^{2+} (Ma and Coronado, 1987, 1988).

Interpretation of anomalous interactions is further complicated by considerations of voltage dependence. At both single- and whole-cell levels, the AMFE between Ba^{2+} and Ca^{2+} has only been reported at depolarized potentials (≥ -10 mV). Interpretation of observations in this potential range is extremely difficult for two reasons, as illustrated by the hypothetical single-ion channel in Fig. 1 (details in Appendix). The values for the free energy profile in the inset of Fig. 1 *A* were chosen to mimic known open-channel current–voltage relations from cell-attached patch recordings with 110 mM [Ca^{2+}] or [Ba^{2+}] in the pipette. Note first that, because the reversal potential with Ca^{2+} as the external charge carrier is larger than with Ba^{2+}, while the inward conductance with Ca^{2+} is smaller than with Ba^{2+} (Hess et al., 1986), current–voltage relations corresponding to various mixtures of extracellular Ba^{2+} and Ca^{2+} converge upon each other at positive potentials. Fig. 1 *A* plots three current–voltage relations corresponding to Ba^{2+} mole fractions of 0 (*a*, 110 mM [Ca^{2+}]), 0.7 (*b*, 77 mM [Ba^{2+}] + 33 mM [Ca^{2+}]), and 1 (*c*, 110 mM [Ba^{2+}]). The differences at positive potentials are minuscule. Hence, even if the channel were a simple single-site pore, slight shifts in voltage control, or in the cell resting potential in the case of cell-attached patches, could deceptively give the appearance of an AMFE. More importantly, Fig. 1 *B* reveals that at voltages ≥ -10 mV, an increasing amount of outward K^+ flux (+) competes with inward Ba^{2+} flux (◊) in determining net current (*solid line*). At these potentials, the relative currents at different mole fractions reflect not only divalent ion permeation, but also K^+ occupancy of the channel. Conductance determinations in solutions of symmetrical divalents (Fig. 1 *C*, ◊), if experimentally accessible, would provide the clearest test of its mole-fraction dependence, but most measurements have been performed under asymmetric conditions with three permeant ions present. Analytical proofs that single-ion channels cannot produce an AMFE have not been derived for the case of three types of ions vying for occupancy of the pore, and it is not clear whether this rule holds under all such situations.

Because of these concerns, we tested for an AMFE between Ba^{2+} and Ca^{2+} at the single-channel level, under conditions where differences between multi- and single-ion behavior would be unambiguous. We recorded unitary currents through L-type Ca channels in guinea pig ventricular myocytes, the same preparation in which an AMFE was found at the whole-cell level by Hess and Tsien (1984) and by McDonald and co-workers (1986). Because of the constraint of asymmetrical ionic conditions entailed by the cell-attached configuration (required to avoid loss of activity with

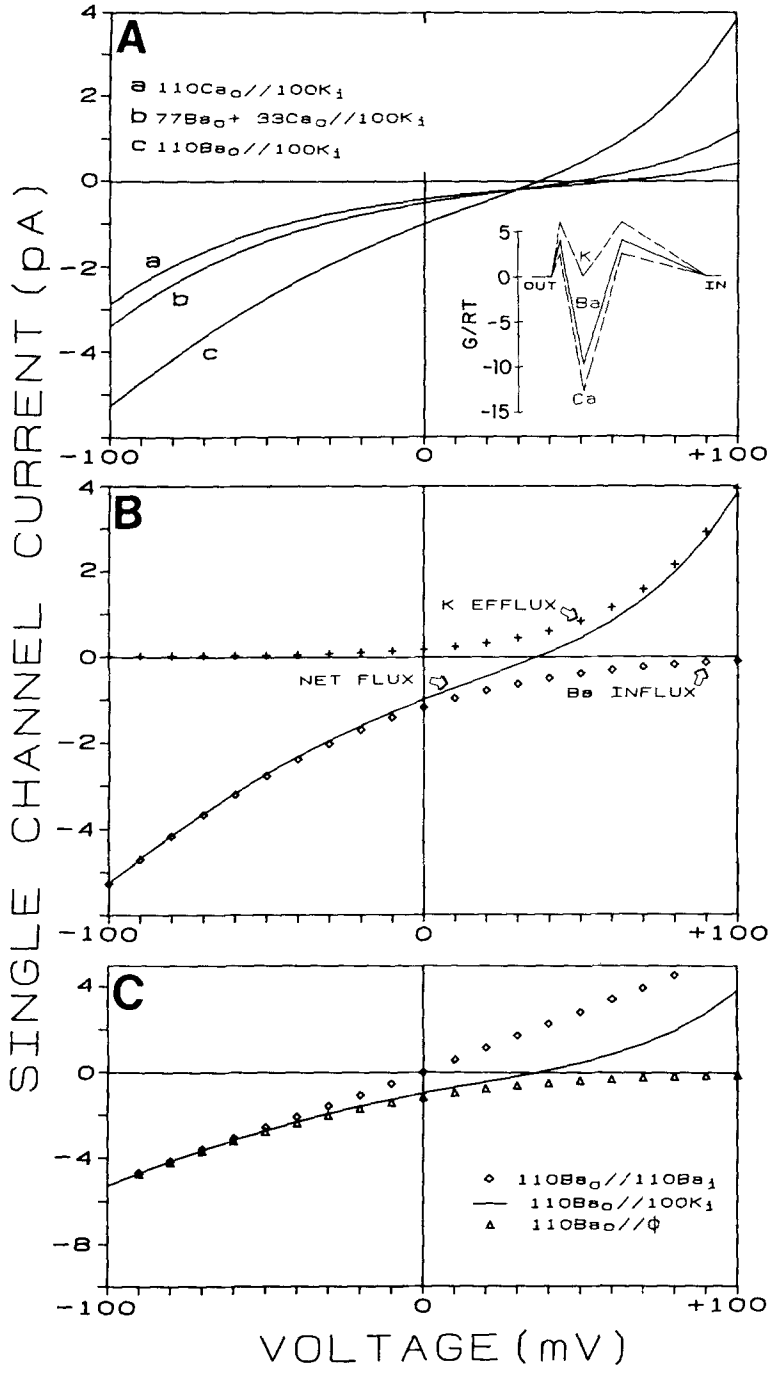
A
a 110Ca$_o$//100K$_i$
b 77Ba$_o$+ 33Ca$_o$//100K$_i$
c 110Ba$_o$//100K$_i$
a
b
c
G/RT
OUT
IN
K
Ba
Ca
B
K EFFLUX
NET FLUX
Ba INFLUX
C
110Ba$_o$//110Ba$_i$
110Ba$_o$//100K$_i$
110Ba$_o$//ϕ
SINGLE CHANNEL CURRENT (pA)
VOLTAGE (mV)
-100
0
+100

FIGURE 1

patch excision [Cavalie et al., 1983; cf. Kameyama et al., 1988]), we concentrated primarily on patch potentials between −20 and −80 mV. Focusing on this range of potentials had three important advantages: (*a*) the rank order of conductance at various mole fractions would be clear-out (Fig. 1 *A*); (*b*) K^+ efflux would likely contribute negligibly to the behavior of the channel (Fig. 1 *B*); and (*C*) current–voltage relations, derived from the arrangement of extracellular divalents pitted against intracellular K^+, should mimic those that would be measured with symmetrical divalents (Fig. 1 *C*, ◇) or with extracellular divalents as the only charge carriers (Fig. 1 *C*, △), thereby simplifying the interpretation of our data. Using this strategy, we detect no AMFE between Ba^{2+} and Ca^{2+} at the single-channel level, even when the electrochemical gradients match those in previous studies of macroscopic currents that gave the opposite result. Nevertheless, by measuring unitary channel conductance as extracellular Ba^{2+} activity is varied over three orders of magnitude, we discovered alternative evidence for multi-ion occupancy of the Ca channel, inconsistent with simple allosteric models for L-type Ca channel permeation. Preliminary reports have appeared (Yue and Marban, 1987, 1988b; Marban and Yue, 1989).

MATERIALS AND METHODS

Ventricular myocytes were enzymatically dispersed and suspended in a working solution of the following composition (in millimolar): 120 K glutamate, 25 KCl, 2 $MgCl_2$, 10 HEPES (adjusted to pH 7.4 with KOH at 22°C), 5 K_2H_2EGTA, 10 glucose. The exact technique used for cell isolation follows that detailed by Yue and Marban (1988a), except that adenosine (formerly used to promote coronary vasodilation, but no longer deemed valuable) was omitted. In a minority of the experiments, Ca adenosine triphosphate (ATP, 0.5–1 mM) or 8-bromo-cyclic adenosine monophosphate (8-Br-cAMP, 1 mM) was added to the bath to increase the probability of finding a functional channel in the patch. Neither ATP nor 8-Br-cAMP appeared to influence the open-channel current properties, consistent with previous observations (Yatani et al., 1978; Reuter et al., 1982). The presence of isotonic K^+ in the bath served to zero the resting potential (Marty, 1981; Hess et al., 1986), but only approximately. Even with this maneuver, we found that cells often maintained a membrane potential of ±10 mV or less, and rarely even ±15 mV; this was generally unimportant, since we emphasized conductance measurements rather than absolute current amplitude. In experiments in which the absolute patch potential was critical (as in comparisons of single channel-current at depolarized potentials in 10 mM [divalent]; see Figs. 4 and 6), a slow (~10 mV/s) voltage ramp (Yellen, 1982) was applied to identify the imposed potential at which no leakage current crossed the patch; this was taken as the true 0 mV, and all records corrected accordingly. In any given patch this value remained stable over recording periods of 10–60 min.

FIGURE 1. Hypothetical single-site model for the L-type Ca channel. (*A*) Current–voltage relations predicted by the model for 110 Ca (*a*), 77 Ba + 33 Ca (*b*), and 110 Ba (*c*), with 100 K as the only permeant ion on the inner face of the membrane in all cases. (*Inset*) Free energy profiles for K, Ba, and Ca, with peaks and binding sites located 0.05, 0.2, and 0.45 of the way across the membrane field (from out to in). The free energy values (G/RT units) for the barriers and wells, respectively, are: 6, 0 (K); 4, −9.8 (Ba); 2.5, −12.75 (Ca). (*B*) Deconvolution of the net current in 110 Ba_o/100 K_i (−) into components of Ba influx (◇) and K efflux (+). At positive potentials, K efflux contributes significantly to the net current. (*C*) Comparison of current–voltage relations predicted in symmetrical 110 Ba (◇) vs. asymmetrical arrangements of 110 Ba_o/100 K_i (−) or 110 Ba_o with no internal permeant ion (△).

To measure single-channel currents with high concentrations of various ions in the pipette (e.g., up to 400 mM $BaCl_2$, or 600 mM TEA-Cl), we were challenged by the tendency of patches to rupture soon after seal formation due to the great difference in osmolarity between the pipette (1.2 osM) and the cell interior (~300 mosM). We overcame this problem by bathing the cells in hypertonic solution containing the usual constituents at two- to three-fold their normal concentrations (Yue et al., 1989). This produced no apparent morphologic damage to the cells and often yielded stable cell-attached recordings for periods of 45 min or longer.

As in previous single-channel studies of permeation in L-type Ca channels (Hess et al., 1986; Lansman et al., 1986; Prod'hom et al., 1987; Pietrobon et al., 1988), we took advantage of the ability of dihydropyridine agonists to promote long-lived openings. Thus, we routinely added Bay K 8644 (1–5 μM; Miles Pharmaceuticals, West Haven, CT) to the bath to facilitate full resolution of current amplitudes with no apparent effects on permeation (Hess et al., 1984, 1986). The use of Bay K 8644 had the added advantage that L-type channels could be easily distinguished from T-type channels (observed in <5% of patches) by their characteristically long openings (Nilius et al., 1985). Despite the presence of Bay K 8644, openings were considerably shorter when Ca was the sole permeant cation (mean open times ~2 ms at 0 mV). Nevertheless, even with Ca as the sole divalent cation, the identity of Ca channel types was unambiguous: the open time distributions for L-type channels were distinctive in their biexponential nature and in their longer mean open times; T-type channels demonstrated monoexponential open time distributions with mean values $\leq$0.8 ms at similar voltages (S.W. Herzig and D.T. Yue, unpublished observations).

Data Collection and Analysis

We used a commercially available patch clamp amplifier (Axopatch 1B with CV-3-1A headstage, Axon Instruments, Inc., Burlingame, CA) to collect data in the cell-attached, single-channel configuration, with pipettes manufactured from borosilicate glass and insulated with Sylgard (Hamill et al., 1981). In pilot experiments, we found that pipettes manufactured from Corning 8161 soft-lead glass (Garner Glass Co., Claremont, CA) yielded favorable seals but introduced an unknown blocking ion into the pipette, so that voltage-dependent block similar to that described for Cd^{2+} (Lansman et al., 1986) was spuriously introduced into the records (see also Cota and Armstrong, 1988, and Furman and Tanaka, 1988). This problem was not encountered with pipettes made from borosilicate glass. Data were usually digitized at 10 kHz, filtered at 2 kHz (−3 dB, four-pole Bessel filter), and stored in a computer (Indec 11-73; Indec Systems, Sunnyvale, CA), unless otherwise noted. A smooth leak template fitted to blank sweeps at each potential was subtracted from the records. Records of channel openings were often subjected to a least-squares fit of Gaussian functions to amplitude distribution histograms to render more precise the estimation of unitary current amplitude. Conductance was obtained by regression of the values for i over the (quite linear) range from −20 to −80 mV.

Voltage Protocols

At positive potentials, open state probability was often sufficiently high that a simple depolarizing voltage pulse from a holding potential of −40 to −100 mV sufficed to elicit channel activity. At negative potentials, where the probability of a channel remaining open is much lower, we generally used a tail pulse protocol: channels were opened by a brief (~10 ms) prepulse to 40 or 50 mV, after which the patch was stepped to the desired test potential and the channels were observed before deactivation. Tails were particularly favored in Ca-containing solutions, to enable selection for fully resolved openings in which the square shape of the unitary event was readily apparent. Ramp voltage protocols (Yellen, 1982) were some-

times used when Ba was the predominant permeant ion; in such cases, openings were long enough that current-time trajectories could be easily determined.

Calculation of Divalent Cation Activity Coefficients

The activity coefficient for Ba^{2+} or Ca^{2+}, f_a, was calculated using the Guggenheim extension of the Debye-Huckel equation, along with the "Guggenheim convention" for the conversion of mean to single-ion activity coefficients (see Eqs. 1–4 in Blinks et al., 1982):

$$\log_{10}(f_a) = 2\{bI - (A|Z_+Z_-|\sqrt{I})/(1 + \sqrt{I})\},$$

where Z_+ (2) and Z_- (1) are the valences of the ± ion pair in question; I is the total ionic strength of the solution in molar, including charged ions other than Ba^{2+} and Ca^{2+}; A is an empirical constant equal to 0.51 at 25°C; and b is another empirical constant equal to $0.1\,|Z_+Z_-|$. The activity coefficient for 100 mM [K] was set at 0.6 (Harned and Owen, 1958).

Terminology

For simplicity in the remainder of this paper we will omit the units of mM, the valence, and the brackets when giving specific values for ion concentrations, so that, e.g., 110 Ba will signify 110 mM $[Ba^{2+}]$.

Statistical Analysis

Pooled data are expressed as mean ± standard deviation unless otherwise indicated.

RESULTS

No Anomalous Mole-Fraction Effect at High or Low Divalent Cation Concentrations

We initially determined single-channel current–voltage relations using a high concentration (110 mM) of permeant divalents to maximize signal-to-noise ratios, thereby improving our chances of resolving even small anomalous effects. Fig. 2 shows representative raw current records (*A*) and current–voltage curves (*B*) in 110 Ca, 55 Ca/55 Ba, and 110 Ba. Compare first the two extremes, pure Ca and pure Ba. In agreement with previous results (Cavalie et al., 1983; Hess et al., 1986), unitary Ba currents are bigger at each potential sampled than are the corresponding Ca currents, and the conductances in the linear range between −20 and −80 mV are quite different (9.7 pS vs. 29.1 pS in Fig. 2 *B*). The important finding here comes in the data with mixtures, in which the total divalent cation concentration has been kept at 110 mM: contrary to predictions of an AMFE, the unitary currents in the mixture are no smaller than those in the pure Ca solution. More importantly, the conductance determined at negative potentials, which is a more easily interpretable reflection of the interaction of the channels with divalent ions, is distinctly greater in the 55 Ba/55 Ca mixture than in 110 Ca. Neither current nor conductance yields an indication of anomalous mole-fraction behavior. In fact, the overall behavior would be approximated quite well by the predictions of the single-ion model in Fig. 1 (compare Figs. 1 *A* and 2 *B*).

The findings illustrated in Fig. 2 for mole fractions of 0, 0.5, and 1 are representative of a total of 15 patches at various mole fractions with a total divalent cation

concentration of 110 mM, as shown by the pooled data in Fig. 3. The relationship between mole fraction and conductance is monotonic, with no indication of anomalous behavior at any mole fraction. The meaning of the solid curves that fit the data here and in Fig. 5 is incidental now but will be addressed in the Discussion.

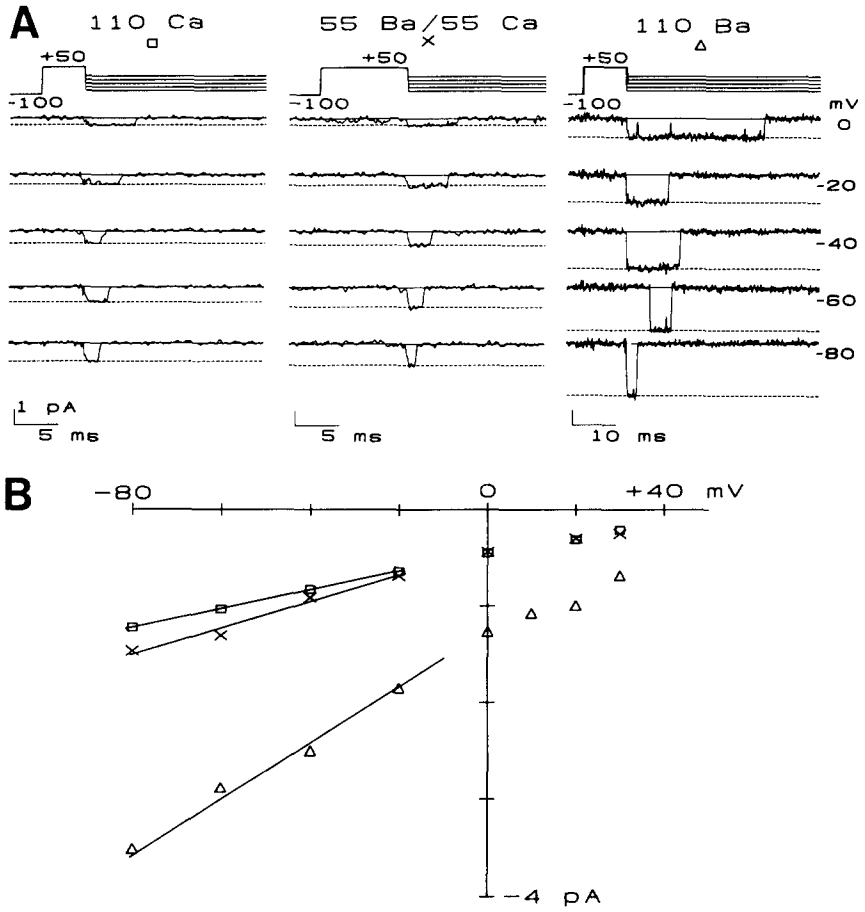

FIGURE 2. Elementary currents in various Ba mole fractions at a high concentration of permeant divalents. (*A*) Voltage protocols and representative current records from patches in 110 Ca (*left*), 55 Ba/55 Ca (*center*), and 110 Ba (*right*). (*B*) Open-channel current–voltage relations from these patches, fitted by lines regressed from −80 to −20 mV, yield conductances of 9.7 pS in 110 Ca (□), 13.2 pS in 55 Ba/55 Ca (×), and 29.1 pS in 110 Ba (△). In addition to the divalent cations above (added as Cl salts), all pipette solutions included 10 HEPES-TEA-OH, pH 7.4.

Despite the absence of an AMFE with divalent concentrations of 110 mM, such a condition might not give a fair chance for some multi-ion channels to display anomalous behavior. If the channel were absolutely saturated by permeant ions throughout the mole-fraction experiment, no anomalous behavior would be observed, as can be shown by simulation (Campbell et al., 1988). Because of this possibility, we

also performed single-channel mole-fraction experiments at a total divalent cation concentration of 10 mM, the same as in the original whole-cell experiments. Fig. 4 shows tail current records (*A*) and current–voltage relations (*B*) obtained with pipette solutions containing 10 Ca, 7 Ba/3 Ca, and 10 Ba (cf. Hess and Tsien, 1984). Even at 0 mV, the long-lasting channel openings can be resolved. As in the experiments with 110 mM divalents, the raw records in Fig. 4 *A* reveal no tendency for unitary currents to decrease when Ba and Ca are mixed. Linear regression of the current–voltage data in Fig. 4 *B* yields conductances of 9.1, 13.6, and 20.7 pS at mole fractions of 0, 0.7, and 1. These patches demonstrate that, even under conditions designed to mimic the original whole-cell experiments, there is no AMFE at the single-channel level. Again, the shapes of this family of current–voltage curves are entirely consistent with those predicted by a single-ion model (Fig. 1 *A*).

Fig. 5 summarizes the results from nine patches and confirms that there is no AMFE in conductance. The nadir of the anomalous effect observed at the whole-cell level centered around mole fractions of 0.7 (Hess and Tsien, 1984; Almers and McCleskey, 1984; McDonald et al., 1986), a finding that contrasts with the single-channel data.

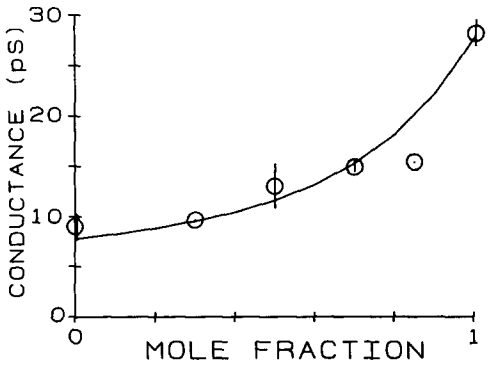

FIGURE 3. Mole-fraction dependence of conductance with total divalent concentrations of 110 mM reveals no anomalous effect. Pooled data show single points from individual patches, or means ± SD when $n = 3$ (at mole fractions of 0, 0.7 and 1) or $n = 4$ (mole fraction of 0.5). The solid curve was predicted by the model in Fig. 9 *C*, assuming 100 K_i. Pipette solutions as in Fig. 2.

There is no indication of an AMFE in conductance here, but what about with current as the parameter of interest? The main purpose of scrutinizing the absolute currents at positive potentials is to facilitate direct comparison with the original whole-cell experiments, not to evaluate whether the channel can be occupied by more than one ion at a time. Small anomalous effects in current at these higher potentials would, in any case, be difficult to interpret mechanistically because of the contribution of outward K flux to the net current (Fig. 1 *B*). At potentials negative to −20 mV, there is clearly no anomalous behavior of the current in Ba/Ca mixtures (Fig. 4 *B*). At voltages ≥ -10 mV, where the original whole-cell experiments were performed, the current-voltage relations converge, but do not appear to cross. Nevertheless, quantitation of the absolute current amplitudes in this range requires some care. Because differences in current might be very small at positive potentials, it is important to recognize and compensate for the slight uncertainty in resting potential which can persist despite the high K in our bath solutions. Toward this end, we took the true 0 mV transpatch potential to be that which resulted in zero

transpatch leakage current (see Methods). This leads to corrections of ±15 mV from the nominally zero potential, which have been incorporated into Fig. 4 and the comparison to follow.

Fig. 6 focuses on the mole-fraction dependence of single-channel current at 0

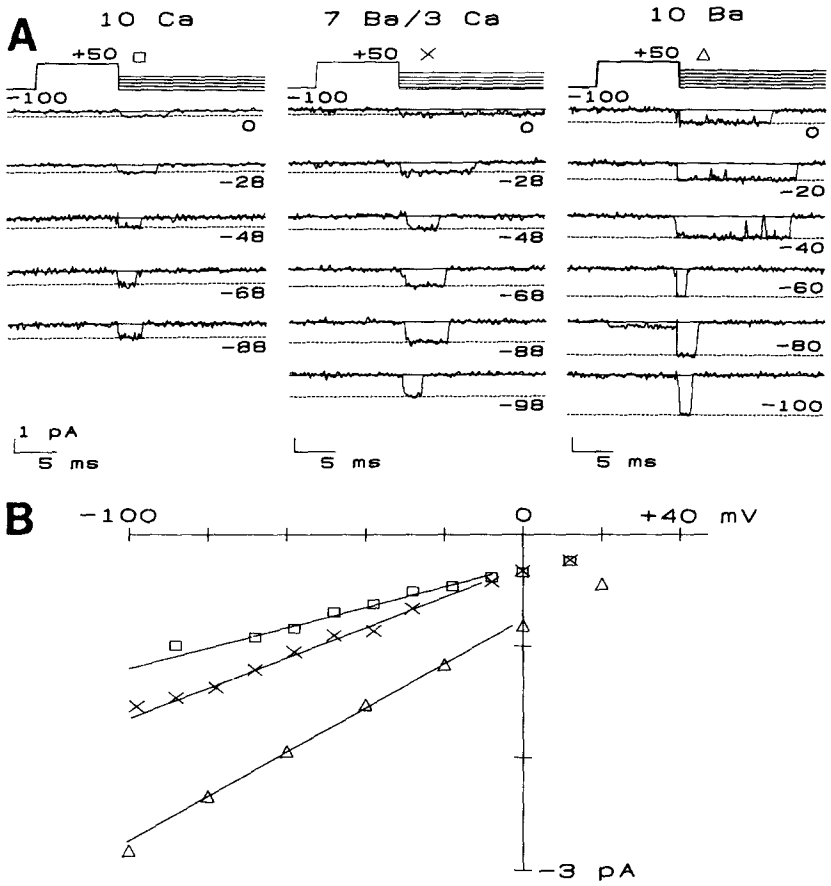

FIGURE 4. Elementary currents at three mole fractions recorded in a total divalent cation concentration of 10 mM. (*A*) Voltage protocols and representative current records from patches in 10 Ca (*left*), 7 Ba/3 Ca (*center*), and 10 Ba (*right*). (*B*) Open-channel current–voltage relations from these patches, fitted by lines regressed from −80 to −20 mV, yield conductances of 9.1 pS in 10 Ca (□), 13.6 pS in 7 Ba/3 Ca (×), and 20.7 pS in 10 Ba (△). In addition to the divalent cations above (added as Cl salts), all pipette solutions included 135 TEA-Cl, 30 sucrose, 10 HEPES-TEA-OH, pH 7.4.

mV, within 3 mV of the membrane potential used in the previous whole-cell fluctuation analysis (when an uncorrected junction potential of 7 mV in the experiments of Hess and Tsien, 1984, is subtracted from the nominal +10 mV; Hess et al., 1986). Since the unitary currents were small, we used histogram analysis to determine the true amplitudes. Slight drifts in leakage current, not noticeable by eye, made it

important to sample segments of data for the histogram analysis according to the following criteria. Well-resolved openings and short segments of bracketing current baselines on both sides were included in the histogram analysis, so that two peaks appear in the histograms, one corresponding to the baseline and the other to current during channel openings. The open-channel current amplitude was then taken as the difference between the medians of two overlapping Gaussian functions fitted to the data by iterative, nonlinear least-squares analysis (Draper and Smith, 1981). In Fig. 6 *A*, representative openings used in the analysis appear to the right of the histograms. That the double Gaussian functions provide excellent fits to the histograms, with few events in the valley between the peaks, attests to the good resolution of open and closed amplitudes free from contamination by filtered gating transitions (Yellen, 1984). The results of such histogram analysis reveal that there is no detectable AMFE even with current at 0 mV as the endpoint: the best fits to the data in Fig. 6 *A* yield current amplitudes of −0.339, −0.345, and −0.856 pA for mole fractions of 0, 0.7, and 1, respectively. Results from a total of nine patches were consistent, as demonstrated by the pooled data plotted in Fig. 6 *B*.

Thus, we conclude that the "anomalous mole-fraction effect" as observed at the

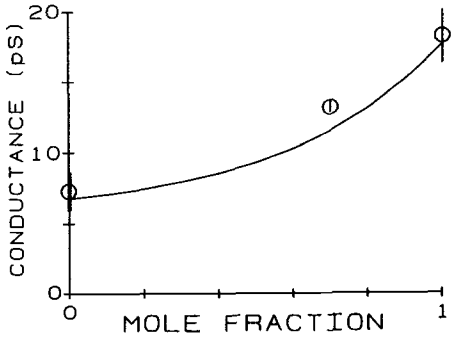

FIGURE 5. Dependence of conductance upon mole fraction at a total divalent concentration of 10 mM. Means ± SD for three patches are shown for mole fractions of 0, 0.7, and 1. The solid curve was predicted by the model shown in Fig. 9 C, assuming 100 K_i. Pipette solutions as in Fig. 4.

whole-cell level does not reflect a property of L-type Ca channel permeation in heart cells.

Alternative Evidence for Multi-ion Occupancy of L-Type Ca Channels

The absence of an AMFE between Ba and Ca weakens the evidence supporting a multi-ion mechanism for permeation. An allosterically-regulated, single-ion channel would suffice to explain many of the remaining properties of Ca channels (Kostyuk et al., 1983; Kostyuk and Mironov, 1986), especially if the regulatory site is situated within the membrane field (but not necessarily in the permeation pathway). To distinguish between single- and multi-ion theories, we adopted a strategy used in the investigation of many enzyme-catalyzed reactions (Piskiewicz, 1977): measurement of turnover rate (conductance) as a function of substrate activity (permeant ion activity). Provided that a sufficiently large range of ion activities can be spanned (Hille and Schwarz, 1978), this approach can produce valuable insight into the binding of ions to sites within the pore.

Until now, patch-clamp recordings of single Ca channels have been restricted to

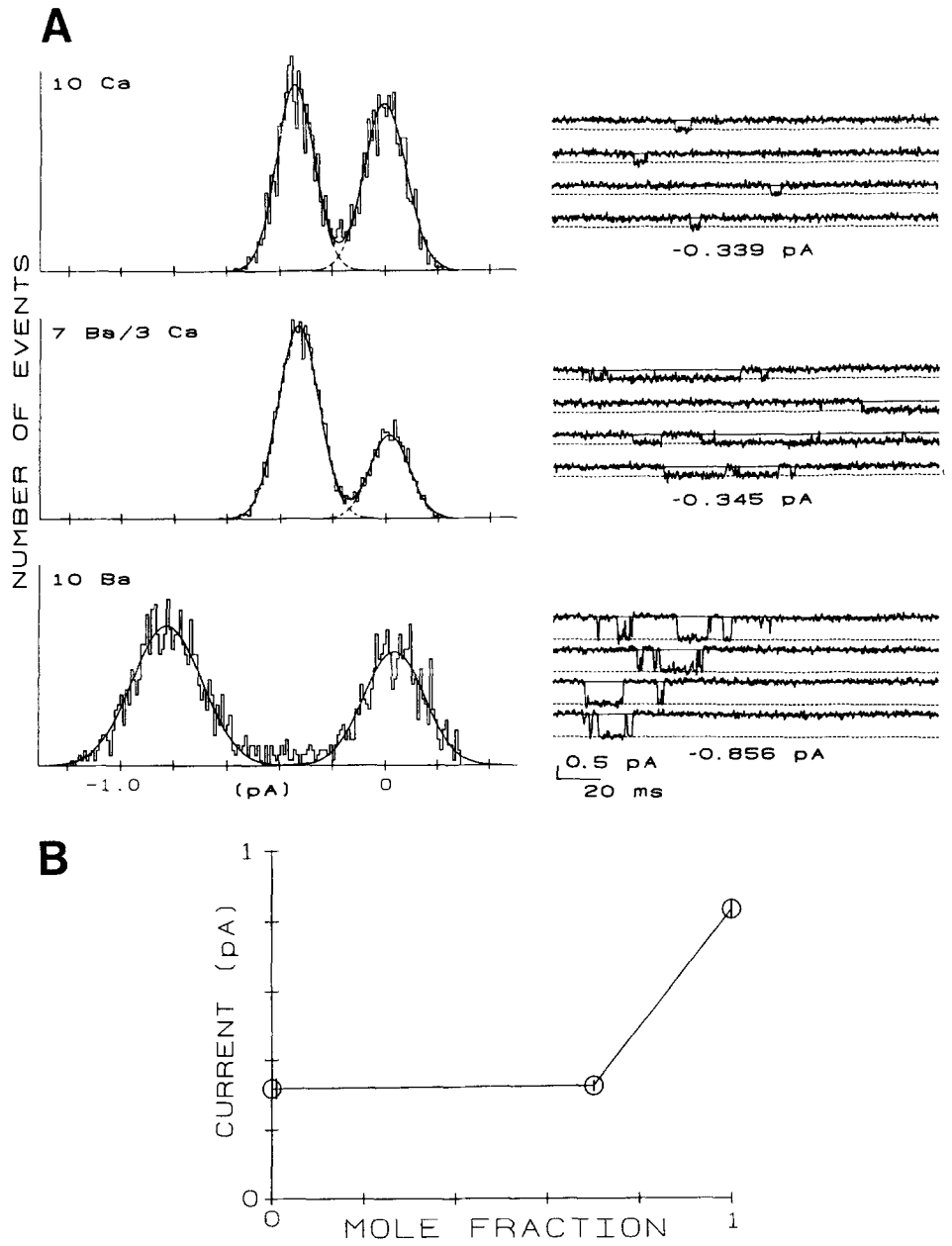

FIGURE 6. Unitary currents at 0 mV as a function of mole fraction with total divalent cation concentration of 10 mM throughout. (*A*) Amplitude histograms optimally fitted by two Gaussian functions (*left*), and typical current records (*right*), in 10 Ca (*top*), 7 Ba/3 Ca (*center*), and 10 Ba (*bottom*). The amplitudes of the channel openings, determined from the differences of the medians of the best-fit Gaussians for the baseline and the open-channel current, equal −0.339 pA (10 Ca), −0.345 pA (7 Ba/3 Ca), and −0.856 pA (10 Ba). (*B*) Mean (± SD) amplitudes of the unitary currents from the same patches as in Fig. 5 (n = 3, each point). Displayed sweeps were all filtered at 1 kHz. Histograms were constructed from sweeps filtered at 1 kHz for 10 Ca and 7 Ba/3 Ca, and from sweeps filtered at 5 kHz for 10 Ba.

permeant divalent concentrations of 10 to 110 mM (Hess et al., 1986); bilayer recordings can extend to higher concentrations, but are hampered by signal-to-noise limitations at the lower end of this concentration range. We found that, without special measures, unitary currents through L-type channels can be resolved with Ba concentrations as low as 1 mM. Furthermore, by bathing cells in hyperosmolar solutions (see Materials and Methods), cell-attached recordings can be obtained with Ba concentrations as high as 400 mM. These innovations allowed us to explore the dependence of conductance on permeant ion activity over a range of activities spanning nearly three orders of magnitude (from 3×10^{-1} to 1.03×10^{2} mM), while working within the constraints of the cell-attached configuration. If the channel pore contains only a single binding site for divalent ions, then the relationship between conductance and symmetrical Ba activity should be well fit by a Langmuir isotherm, as in Michaelis-Menten kinetics (Lauger, 1973; Bell and Miller, 1984). Since our conductance measurements derive from data collected between -20 and -80 mV, they should mimic those which would be obtained with symmetrical Ba for a single-ion channel (Fig. 1 *C*). Hence, the same test for a single-ion channel should apply to our results. Deviations from single-site predictions would suggest that more than one binding site exists, and would provide important empirical constraints for a more realistic permeation model.

Fig. 7 *A* shows single-channel tail current records at voltages from 0 or -10 mV to -100 mV with Ba of 1, 5, and 400. (Note the differences in the scale bars from panel to panel.) The existence of unitary currents large enough to resolve in 1 Ba is unanticipated by either earlier results with noise analysis that predicted much smaller unitary currents at physiological divalent concentrations (Fenwick et al., 1982), or by more recent work that treats the saturation of Ba permeation as a Michaelis-Menten process with an effective K_d of 9.6–27.9 mM (Hess et al., 1986; Ganitkevich et al., 1988; Rosenberg et al., 1988). Open-channel current-voltage relations are plotted in Fig. 7 *B*, along with the best-fit regression lines derived from the points from -20 to -80 mV.

The results of our saturation experiments are summarized in Fig. 8 *A*, which plots conductance vs. Ba activity. Close inspection reveals two features that hint that the relationship is inconsistent with Michaelis-Menten kinetics. Conductance initially rises quite rapidly, with a surprisingly high value of 7.1 pS at 1 Ba (0.3 mM Ba activity). As Ba activity increases, this initial fast rise gives way to a slow, progressive creep in conductance. The lack of clear-cut saturation at high [Ba] has also been observed in L-type channels in bilayers ($K_d \geq 20$ M in Ma and Coronado, 1987; cf. Rosenberg et al., 1988). Deviations from Michaelis-Menten kinetics are even more readily apparent in the Eadie-Hofstee transformation of our data, shown in Fig. 8 *B*. If the pore bound only one ion at a time, the Eadie-Hofstee plot would be linear. Instead, the relationship in Fig. 8 *B* deviates flagrantly from linearity: an attempt to regress one region (high, mid, or low conductance) would fail to fit the two others.

Before interpreting these results in the context of intrapore properties, we considered the possibility that local negative charges near or in the outer mouth of the channel could have enhanced the ion activity facing the entrance of the conduction pathway, particularly at low Ba concentrations. Although ionic strength, and therefore Debye length, was held constant over the concentration range from 1 to 55 Ba, changes in *divalent* cation concentrations are themselves sufficient to alter

surface potential (see, e.g., McLaughlin, 1977, for a treatment of Gouy-Chapman-Stern theory). Such local charge effects could influence the shape of the relationship between permeant ion activity and channel conductance (e.g., Green et al., 1987), as has been shown for monovalent cation permeation through L-type Ca

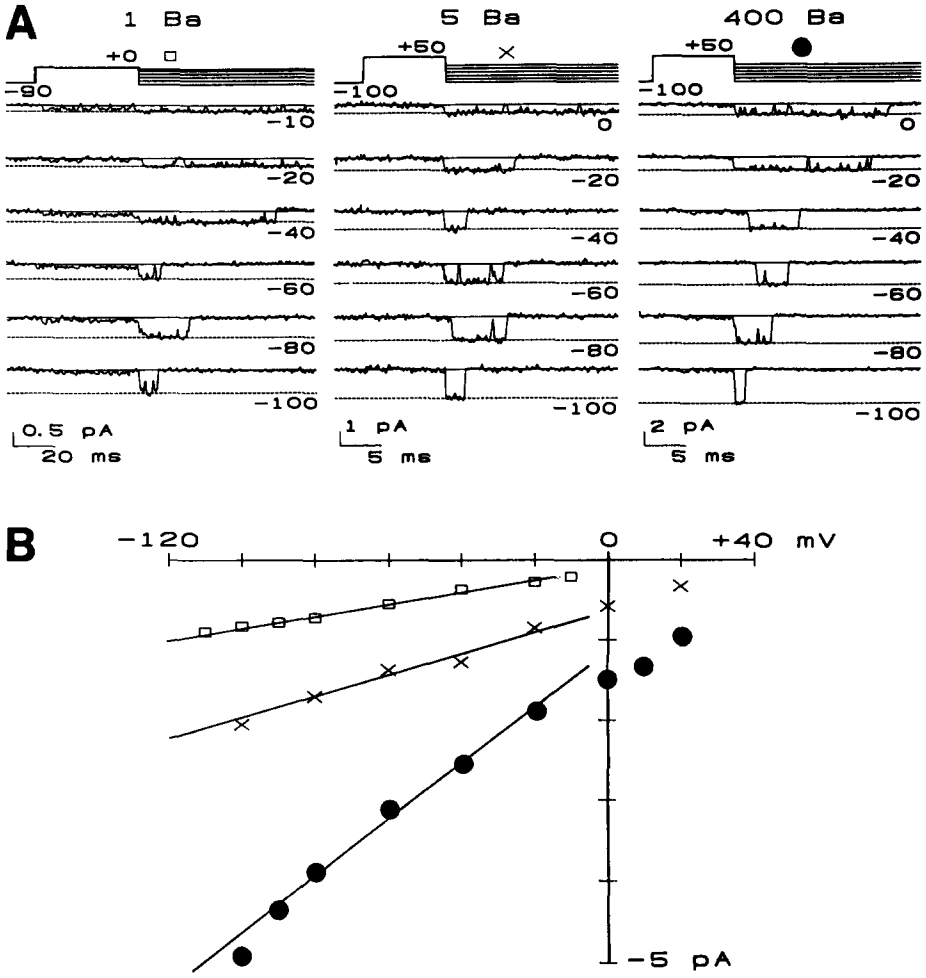

FIGURE 7. Single-channel conductance in three different Ba concentrations. (*A*) Unitary currents in 1 Ba (*left*), 5 Ba (*center*), and 400 Ba (*right*) during pulses to the voltages indicated next to each record. (*B*) Open-channel current–voltage relations from these three patches yield conductances of 7.3 pS in 1 Ba (□), 13.3 pS in 5 Ba (×), and 34.9 pS in 400 Ba (●). Pipette solutions as described in Fig. 8.

channels (Prod'hom et al., 1989). Fig. 8 *C* tests for such a possibility by comparing open channel conduction for pipette solutions in which the ionic strength was adjusted to yield the same Ba activity (1.5 mM), but twofold different Debye lengths. If local negative charges are in fact enriching permeant divalent cation

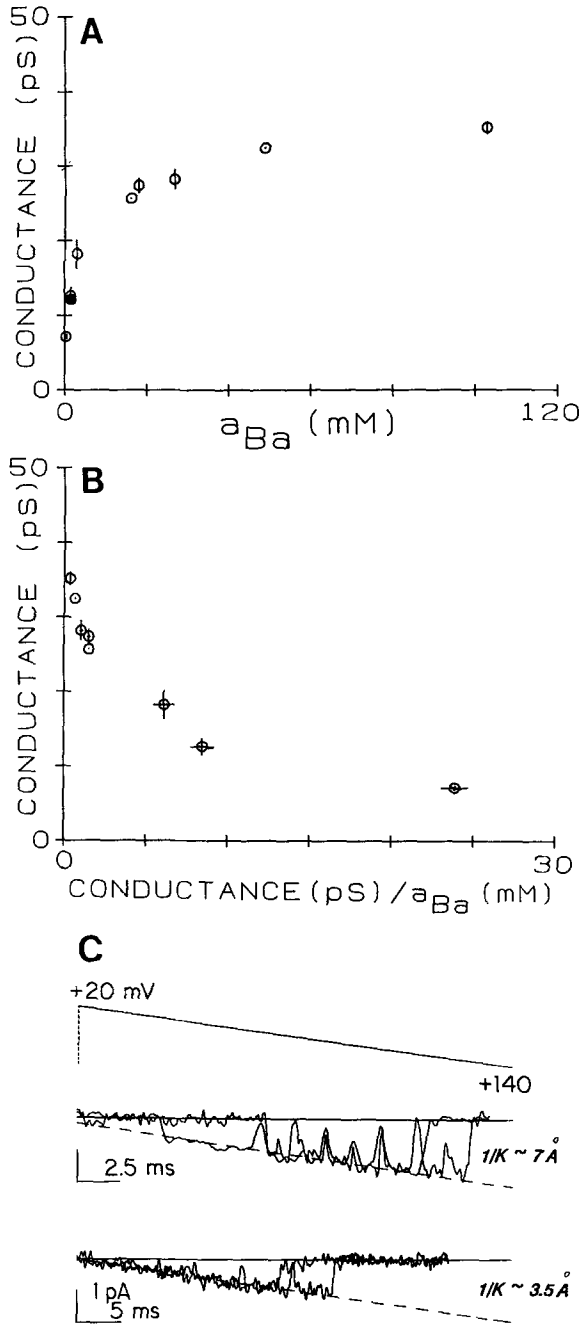

FIGURE 8. Relation of Ba conductance to Ba activity in the L channel channel. (A) Pooled data (*unfilled symbols*) for conductance vs. Ba activity (a_{Ba}); means ± SD are plotted for $n \geq$ three patches, except for the two points without error bars. The filled symbol represents the average of two patches (range less than symbol size) using a pipette solution with one-half the Debye length of the solutions corresponding to the unfilled symbols at the same a_{Ba}. Ionic strength was held constant for points between 1 and 55 Ba, so that the same activity coefficient would apply during this sharply rising, critical phase of the plot, thereby making inferences from this portion of the curve independent of exact knowledge of activity coefficients. For points between 70 and 400 Ba concentrations, activity coefficients were adjusted for varying ionic strength as described in the Materials and Methods. Here, exact knowledge of activity coefficient is less critical because of the shallow rise of the curve; the conductances attained at the higher divalent activities could not be produced by a single-ion model at any (even infinite) activity as shown below in *B*. For the unfilled symbols, the actual activity coefficient equaled 0.299 for [Ba] ≤ 55. In addition to [$BaCl_2$] (1, 5, 10, 55), the pipette solutions with this activity coefficient contained 10 HEPES-TEA-OH (pH 7.4), variable concentrations of TEA-Cl chosen to maintain a constant ionic strength of 170 mM (corresponding to a Debye length of ~7 angstroms), and variable concentrations of sucrose to maintain an osmolarity of ~340 mM. For the remaining four [$BaCl_2$] (70, 110, 220, 400), the activity coefficients were 0.256, 0.243, 0.222, and 0.257, with 10 HEPES-TEA-OH, pH 7.4. The pipette solution corresponding to the filled symbol contained [$BaCl_2$] (6.66 mM, a_{Ba} = 1.5 mM), 600 TEA-Cl, 10 HEPES-TEA-OH, pH 7.4. The resulting ionic strength is ~625 mM, corresponding to a Debye length of ~3.5 Å. (*B*) Eadie-Hofstee transformation of the data in A would have been linear if saturation were a Michaelis-Menten process. Instead, there is clear deviation from linearity at both high and low a_{Ba}. (*C*) Current–time trajectories evoked in response to the voltage ramp protocol diagrammed at top. Both upper and lower sets of traces were obtained with a_{Ba} = 1.5 mM, but corresponding Debye lengths of pipette solutions were about 7 and 3.5 Å, respectively. Segments corresponding to channel openings for both sets of traces have been fit with a 12 pS trajectory (- - -). The extrapolated reversal potential is less positive for the lower set of traces, consistent with the higher bath osmolarity required to maintain seals in this (high ionic strength) pipette solution. Pipette solutions are described in *A*.

activity at the channel mouth, the solution with the shorter Debye length (~3.5 Å; Fig. 8 *C*, *bottom trace*) should yield a lower conductance than that observed at "physiological" Debye lengths (~7 Å; *middle trace*); the sphere of influence of the surface charges would be much smaller in volume. Contrary to this prediction, currents recorded in both Debye lengths during voltage ramps are well fit by 12-pS trajectories (*dashed lines* in Fig. 8 *C*). The mean conductance from two patches with the high ionic strength solution (Fig. 8 *A*, ●) superimposes upon the conductance values obtained at the lower ionic strength (*open symbols*). Surface charge effects would be even smaller at higher divalent cation activities due to increased screening and binding of local charges. The results argue against appreciable local surface charge effects on conduction in our experiments; apparently, the negative charges revealed in the strict absence of divalents (Prod'hom et al., 1989) are neutralized when such cations are present at mM concentrations, consistent with results from L-type Ca channels of muscle reconstituted in bilayers (Coronado and Affolter, 1986). We therefore interpret the deviations from Michaelis-Menten kinetics in Fig. 8, *A* and *B* as direct evidence against permeation mechanisms in which only one ion at a time can bind to the pore.

DISCUSSION

We have demonstrated the absence of an AMFE between Ba and Ca at the single-channel level (Figs. 3 and 5), calling into question the need for a multi-ion permeation scheme. Nevertheless, our finding that conductance does not vary with Ba activity according to Michaelis-Menten kinetics provides new evidence against simple single-ion theories.

Relation to Previous Studies

Our results are at variance with data from L-type channels in PC-12 cells (Friel and Tsien, 1989), in which a small AMFE was detected at voltages positive to −20 mV, under ionic conditions similar to those in our Fig. 6. Small, uncorrected variations in cell resting potential, even in high-K solutions, might have produced the appearance of an AMFE in the PC-12 cells, but it is hard to imagine how such errors could have favored any systematic tendency. Instead, we suspect that the difference may be a genuine biological one between L channels in the two types of cells. Permeation is known to vary quite significantly among L-type channels from different sources (e.g., from cardiac and skeletal muscle: Rosenberg et al., 1986); in fact, our unitary Ba currents (Figs. 2 and 4) appear to be appreciably larger at 0 mV than than those reported for PC-12 cells. Regardless, small anomalous effects in this voltage range would be difficult to interpret mechanistically due to the confounding contribution of outward K flux (Fig. 1 *B*). Conductance at negative membrane potentials, which is a more straightforward indication of divalent ion occupancy, fails to demonstrate an AMFE even in PC-12 cells (see Fig. 4, Friel and Tsien, 1989). Other, non-L types of Ca-permeable channels, such as those described by Chesnoy-Marchais (1985) in *Aplysia* neurones, can exhibit an unambiguous AMFE between Ba and Ca, at least under tri-ionic conditions at positive potentials. The contention that these channels are not L type is suggested by the following observations: their conductance in pure Ca or Ba is four times greater than described for dihydropyri-

dine-sensitive channels; the mean open times are much longer in Ca than in Ba, opposite to the gating behavior characteristic of L-type channels (Cavalie et al., 1983); they are relatively insensitive to block by Cd, with a $K_{1/2}$ some two orders of magnitude higher than for L-type channels (cf. Lansman et al., 1986); Mg is quite permeable, again in contradistinction to L-type channels (Hess et al., 1986); and finally, the channels of Chesnoy-Marchais (1985) demonstrate no inactivation, either with Ba or with Ca as the charge carrier (cf. Mitra and Morad, 1986).

If the AMFE described previously with cardiac macroscopic currents is not a property of permeation, gating must be altered in some unanticipated manner when Ba and Ca are mixed. We did note a tendency for mean open state probability to be lower in divalent cation mixtures as compared to the pure solutions, due primarily to an increase in the frequency of blank sweeps. However, such differences were not statistically significant due to the large variability in absolute open state probability among patches. We have no further insight regarding the possible origin of such a paradoxical effect, other than to note the protean effects of divalent cations on channel gating in a variety of different cell types (e.g., cardiac Ca channel inactivation [Lee et al., 1985]; squid K channel gating [Armstrong and Lopez-Barneo, 1987]).

We now turn our attention to three questions of more general interest raised by our results: (*a*) What is the evidence now favoring a multi-ion permeation mechanism? (*b*) If a multi-ion scheme is necessary, how must it be configured to account for the absence of an AMFE between Ba and Ca? (*c*) Finally, can we estimate from our data the number of binding sites in the L-type Ca channel?

Evidence for a Multi-ion Permeation Mechanism

Several central features of L-type Ca channel behavior must be explained by a good model of ion permeation: (*a*) large monovalent fluxes in the absence of divalents (Kostyuk et al., 1983); (*b*) voltage-dependent block of monovalent fluxes by micromolar concentrations of divalent cations (Lansman et al., 1986); (*c*) acceleration of unblock times by increasing permeant ion concentration (e.g., relief of Cd block by increasing [Ba]; Lansman et al., 1986); and (*d*) non-Michaelis-Menten kinetics in the relation of conductance vs. Ba activity (present study). The two simplest types of models that can explain many of these features are single-ion channels modulated allosterically by a divalent cation binding site (Kostyuk et al., 1983) and multi-ion, single-file channels (Hess and Tsien, 1984; Almers and McCleskey, 1984). How well can either of these models account for these features?

(a) Monovalent ion permeability in absence of divalents. This finding can be explained by either model. For the allosteric case, an empty divalent cation regulatory binding site leaves the channel in a monovalent-permeable conformation. For multi-ion models, the absence of divalent ions in the pore allows monovalents ready access to low-affinity binding sites (with consequently high conductance), sites from which monovalent ions are usually excluded by electrostatic repulsion if a divalent ion inhabits the pore.

(b) Voltage-dependent block of monovalent currents by low concentrations of divalents. The voltage dependence cannot be explained by the bare-bones allosteric model, in which the high-affinity divalent binding site is situated outside the membrane field.

However, if this site were located within the field, its apparent affinity for divalents could be influenced by voltage. Micromolar concentrations of divalent ions would then bind to the allosteric regulatory site in a voltage-dependent fashion and convert the channel into its monovalent-impermeant state, thereby chopping the current and giving the appearance of block. In a multi-ion scheme, divalents bind avidly to deep free energy wells so that, when present in low concentrations, they can bind to the pore with sufficient affinity to impede monovalent flux, but produce little current of their own without the added boost provided by multi-ion occupancy and electrostatic repulsion.

(c) Relief of block by increasing permeant ion concentration. The finding that lifetime of block by one ion is shortened by increasing the concentration of another, more permeant ion is most readily explained by a multi-ion model. As a specific example, there is no ready mechanism in the Kostyuk formulation to account for the observed acceleration in the Cd unblock rate by increasing Ba concentration (Lansman et al., 1986). Nevertheless, the fact that saturation of the relief of block was never observed, even at high [Ba], means that a single-site model with the property of "knock-on" (i.e., displacement and immediate replacement of one ion in the site by another) cannot be excluded (Yellen, 1984). In multi-ion channels, no special pleading is required to explain the relief of block by permeant ions: the departure of a blocking ion can be hastened by a permeant ion occupying an adjacent site and repelling the blocker (Lansman et al., 1986). While this phenomenon favors a multi-ion channel, it does not conclusively necessitate such a scheme, nor does it offer easy clues to glean further insight into the permeation mechanism.

(d) Saturation kinetics. The new data presented here constitute clear evidence in favor of multi-ion occupancy. The Kostyuk model cannot explain non-Michaelis-Menten concentration-dependence of the sort revealed in Fig. 9. After Ba activity exceeds the micromolar range, the allosteric modulatory site should be permanently occupied so that channel conductance should saturate as a simple Michaelis-Menten process. Such behavior was not observed. On the other hand, multi-ion channels predict complicated saturation kinetics, the exact features of which are determined by the number of binding sites and by details of the free energy profile, as will be discussed below.

Multi-ion Channels: Behavior in Mixtures of Ba and Ca

Multi-ion channels can exhibit an AMFE, but are not obliged to do so (Hille and Schwarz, 1978). In fact, we have just reasoned that the L-type Ca channel can accommodate several ions simultaneously despite the absence of an AMFE. Clearly, revision of the Hess and Tsien (1984) or Almers and McCleskey (1984) models, with their prediction of a strong AMFE between Ba and Ca, will be required in order to accommodate the present observations. What features of multi-ion channels determine the presence or absence of such an effect?

To address this question, and those in the section to follow, simple multi-ion models based on Eyring rate theory suffice. Although such formalisms probably oversimplify the dynamics within a biological protein, they do provide a convenient approximation to a complicated diffusion process that might be more realistically described by general rate constant models (Cooper et al., 1988). Here, we employ Eyring sim-

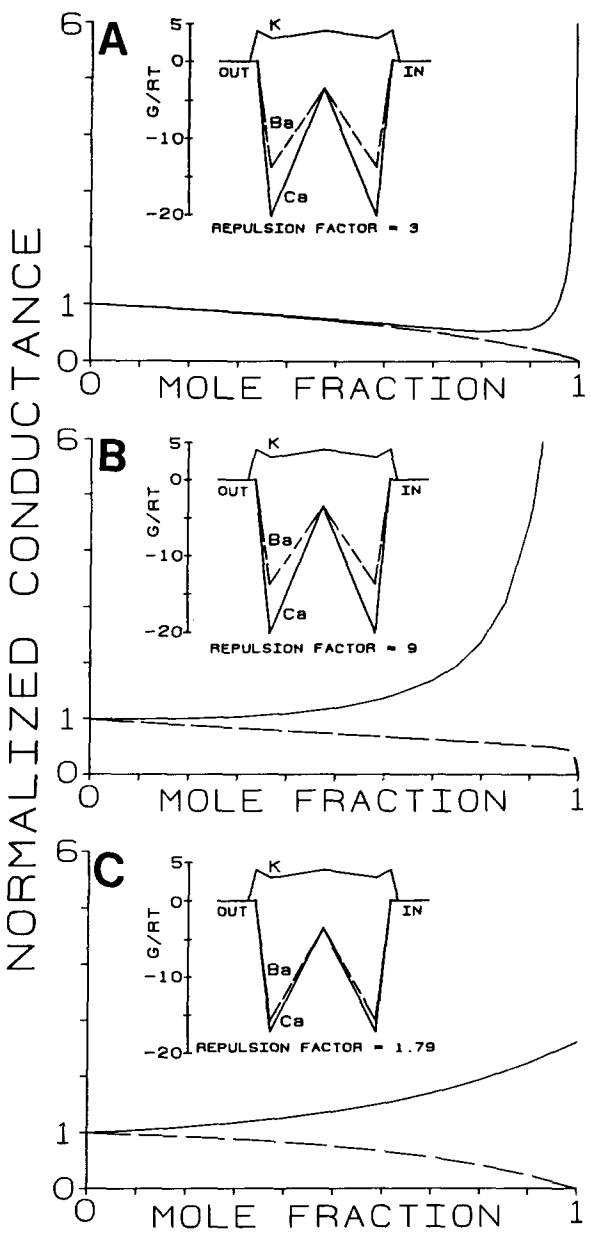

FIGURE 9. Two-ion models and the features which determine their conductance in mixtures of Ba and Ca. In each panel, the symmetrical free energy profiles for K (—), Ba (- - -), and Ca (—) are depicted as insets within a plot of the predicted conductance between −20 and −80 mV as a function of Ba mole fraction, normalized to the conductance at a mole fraction of 0. The entry and exit barrier heights are equal for each cationic species, as are the wells. Peaks and valleys are arranged at 0.05, 0.1475, 0.5, 0.8525, and 0.95 of the way across the membrane field. In *C*, the free energy values (*G/RT* units) at 0 mV for the bracketing barriers, wells, and intermediate barrier are, respectively: 4 (*GPK*), 3 (*GK*), and 4 (*GMK*), for K; 0.1 (*GPB*), −15.79 (*GB*), and −3.5 (*GMB*), for Ba; along with 0.03 (*GPC*), −17.2 (*GC*), and −3.5 (*GMC*) for Ca. In *A* and *B*, all profiles are the same except that the wells for Ba and Ca, respectively, are −13.79 and −20.2. The dashed lines indicate the conductance derived from Ca flux. The simulations assume 10 [Ba + Ca] outside and 100 $[K]_i$. (*A*) The Ba and Ca well depths here are separated by 6.41 *G/RT* units, and the repulsion factor (*F*) equals 3. The model resembles that of Hess and Tsien (1984) when the original formulation is recast in light of the dimensional considerations in the Appendix. (*B*) The chemical terms of the free energy are unchanged from A, but the repulsion factor is 9. (*C*) The Ba and Ca well depths are now separated by only 1.4 *G/RT*, and the repulsion factor is moderately reduced to 1.79.

ulations to distinguish among broad classes of permeation models, while cautioning against overinterpretation of the precise physical implications of such models.

Fig. 9 shows three sets of free energy profiles, each with two symmetrical wells corresponding to ion binding sites (see Appendix for details). Each panel depicts the free energy changes that would be encountered by a K, Ba, or Ca ion as it traverses the channel at 0 mV. Under each free energy diagram is the value of the electrostatic repulsion factor (which would equal 1 with no interaction between the two sites, after Hille and Schwarz [1978]). Finally, the predicted dependence of conductance, calculated between −20 and −80 mV, on mole fraction is depicted in each panel. Only Fig. 9 *A* exhibits an AMFE. This arises because the well depths for Ba and Ca are far apart energetically. Imagine the effect of adding some Ca when the Ba mole fraction is near 1. Because Ca binds avidly (its energy wells are deep), it dwells comfortably in the channel, but in so doing it effectively inhibits occupancy by anything other than a second Ca ion. Ba ions that come in are most often repelled back. Until the probability of another Ca entering the channel is sufficiently high to favor Ca-Ca occupancy (i.e., a low Ba mole fraction), the first Ca ion will tend to remain in the pore and thus will effectively block Ba flux while itself contributing nothing to net current (dashed lines indicate the conductance attributable to Ca ion flux). Hence, the anomalous behavior in mixtures of Ba and Ca.

There are two general ways in which the anomalous effect in Fig. 9 *A* can be abolished. The first involves making the repulsion factor much higher, so that electrostatic interaction becomes the dominant factor which determines whether a channel will be occupied by any two ions simultaneously (Fig. 9 *B*). A very high repulsion factor makes it unlikely that two ions of any species can simultaneously occupy the channel, in effect creating a single-ion pore. But such a channel would be ill suited to carry current (Hille and Schwarz, 1978); the half-saturating point of conductance vs. permeant ion concentrations would occur at much higher activities than predicted by our data (Fig. 8).

Another, more attractive means of abolishing the AMFE involves minimizing the difference in chemical free energy between Ba and Ca. Fig. 9 *C* shows the consequences of moving the well depths for Ba and Ca closer together. There is no queer interaction between Ba and Ca, since they look quite similar to the channel (but dissimilar enough to explain the difference in conductance between pure Ba and pure Ca). Here ion–ion repulsion is not so high as to impede flux at mM concentrations. This particular model, which describes many of our findings, was determined by first fitting the conductance vs. Ba activity data to constrain the Ba wells (Fig. 10 *B*), then fitting the 10 Ca and 110 Ca current–voltage relations to constrain the Ca wells. Once these fits were optimized, the model naturally predicted the mole-fraction behavior in Figs. 3 and 5. In fact, the solid lines in Figs. 3 and 5 are both derived from the model depicted in Fig. 9 *C*.

Thus, the implication of no anomalous mole-fraction behavior is that the Ca channel is the sort of multi-ion pore in which the Ca and Ba binding depths are not very dissimilar energetically.

Number of Binding Sites in the Permeation Pathway

Although two-site models suffice to illustrate the mole-fraction behavior of multi-ion channels, they fail to predict the "creep" in the conductance vs. Ba activity rela-

tion (*shaded region,* Fig. 10 *B*). In fact, this deficiency provides an important clue that there may be more than two binding sites in the channel. Hille and Schwarz (1978) demonstrated that an *n*-site model can produce up to *n* rising phases in conductance vs. activity plots (e.g., their Fig. 6). First, second, and third rising phases correspond to single-, double-, and triple-ion occupancy of the channel. Because singly occupied channels produce flux too small to measure (necessary to explain *block* of monovalent currents by micromolar concentrations of divalent cations), our double-site model produces only one identifiable rising phase (Fig. 10 *B*), corresponding closely to the increasing population of doubly occupied channels (Fig. 10 *A*). Thus, any two-site model is doomed to provide a poor fit to the data in Fig. 10 *B*

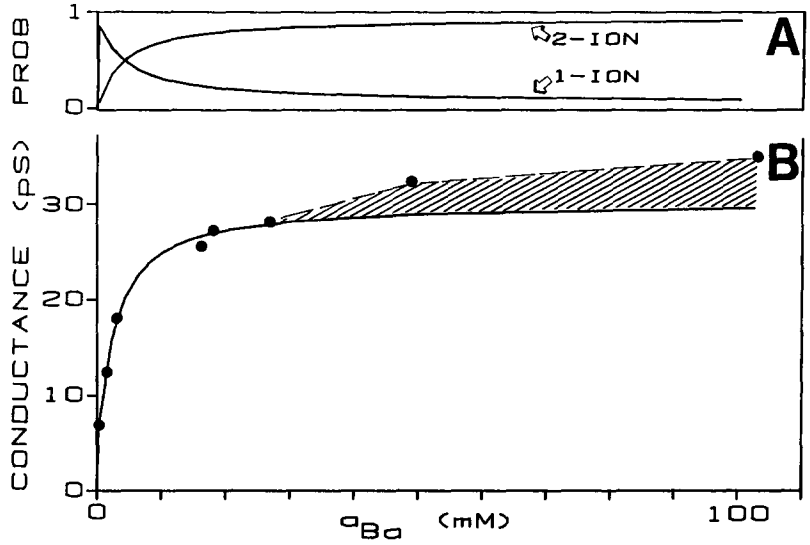

FIGURE 10. Characteristic inability of two-site model (Fig. 9 *C*) to describe adequately the saturation kinetics of single L-type channels. Plots of calculated average ion occupancy per channel (*A*) and single-channel conductance between −20 and −80 mV (——, *B*) as a function of Ba activity. Also shown in B (●) are the measured mean values for single-channel conductance, replotted from Fig. 8 *A*. The model predicts a systematically lower single-channel conductance at high a_{Ba} than observed empirically, as highlighted by the darkened area between the theoretical curve and the actual data. (*C*) Despite this crucial failure of the model in *B*, it predicts quite well many features of the channel, including the mole fraction relations in Figs. 3 and 5.

because nowhere in its repertoire of behavior can it account for an additional rising phase.

The natural implication of the discrepancy between the saturation data and the two-site model predictions (Fig. 10 *B*) is that there are three or more binding sites in the permeation pathway. Although this proposal does not follow necessarily from our results, it is a conclusion that fits our observations quite simply and economically. Fig. 11 demonstrates that a three-site model (*A*, *inset*), formulated as described in the Appendix, provides an excellent fit to the saturation data (*A*, *lower panel*). The upper panel of Figure 11 *A* shows that, as expected, rapid two-ion occupancy pro-

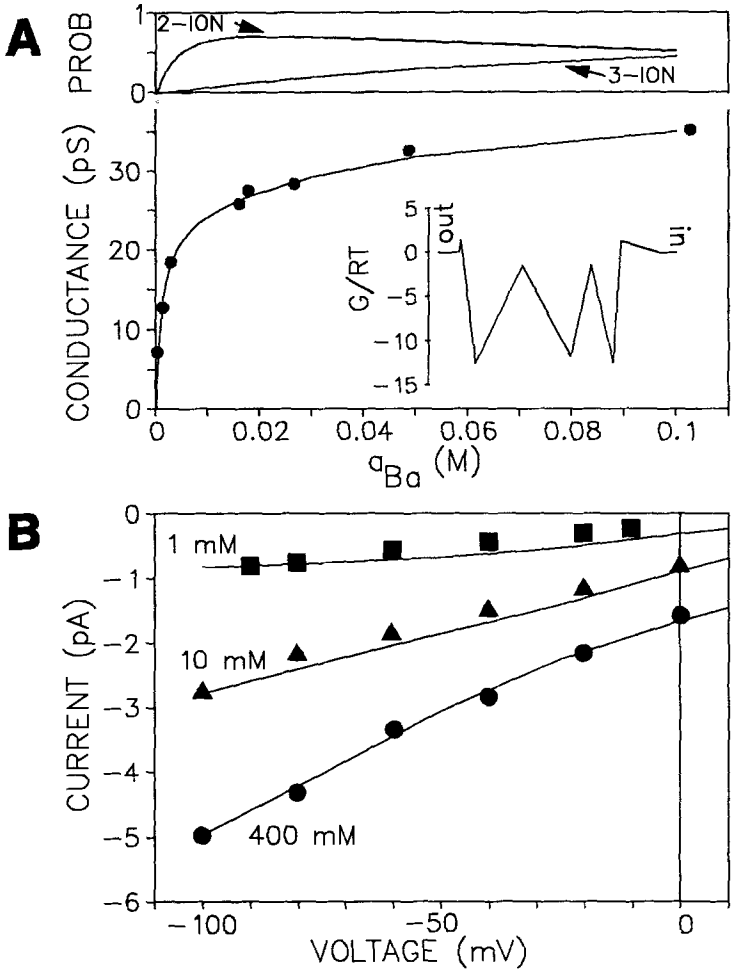

FIGURE 11. Three-site, triple-occupancy model of the L-type Ca channel. (*A*) The calculated mean ion occupancy per channel (*top*) and single-channel conductance between −20 and −80 mV (*bottom*: ——, prediction; ●, data replotted from Fig. 8 *A*). The inset shows the free energy profile for Ba at 0 mV. The free energy values (*G/RT* units) for the bracketing and intermediate barriers are, from outside to inside: 1.3, −1.5, −1.5, and 1.3. The values for the wells are, from outside to inside: −12.46, −11.75, and −12.46. Peaks and wells are arranged at 0.01, 0.08, 0.321, 0.562, 0.6705, 0.779, and 0.822 of the way across the membrane field. The electrostatic repulsion terms are now quite complicated in that interaction among the three sites must be considered; the formulation used here is described in the Appendix. For simplicity we have assumed that over the voltage range that our data concern, we can approximate the triple-site channel behavior by considering only extracellular Ba, and ignoring intracellular K. This greatly simplifies the computation necessary to manipulate the model. (*B*) Observed open-channel current-voltage data in 1, 10, and 400 Ba (symbols) and the predictions of the model (——).

duces the brisk rise in conductance at low Ba activities, while a slower rise in three-ion occupancy yields the gentle secondary "creep" in conductance.

Several other features of the three-site model are noteworthy. The predicted current–voltage relations are in reasonable agreement with those recorded over a broad range of permeant ion concentrations (Fig. 11 *C*). The small electrical distance for the outer entry barrier is consistent with the empirical observations that extracellular entry by divalents into the channel is voltage-insensitive (Lansman et al., 1986), and that the current–voltage relations are nearly linear between −20 and −100 mV (e.g., present study). The modest degree of asymmetry would be consistent with preliminary reports of asymmetrical block of the smooth muscle Ca channel by Cd (Huang et al., 1989). Finally, the model successfully anticipates the large fluxes observed at low permeant divalent cation concentrations.

The L-type Ca channel may not be alone with regard to such a high number of binding sites. Neyton et al. (1988) have recently provided strong evidence for four or more binding sites in the permeation pathway of the high-conductance, Ca-activated K^+ channel from skeletal muscle. As the structures of the cardiac Ca (Mikami et al., 1989) and other channels are elucidated, one of the next major challenges will be to understand how so many cations might be accommodated harmoniously within the conduction pathway.

APPENDIX

The application of Eyring rate theory to ion channel permeation is well summarized elsewhere (Hille and Schwarz, 1978; Begenisich and Cahalan, 1980); only the distinctive features of our modelling will be described here.

Dimensional Considerations at Channel–Solution Interfaces

The first is our approach for handling dimensions. Eyring rate theory does not relate rate constants governing ion entry into the channel and free energy entry barriers. Such rate constants require dimensions of $M^{-1}s^{-1}$, while the dimension of the rate constants provided by Eyring rate theory is s^{-1} (Eq. A-2). This limitation of Eyring rate theory was stated by Hille and Schwarz (1978), so that those authors made no attempt to predict absolute flux values from ion activities in moles/liter. Subsequent Eyring-based models of Ca channel permeation have proceeded to predict the relation between absolute flux and ionic activity without compensating for this dimensional consideration (e.g., Fig. 4 in Hess and Tsien, 1984; Eqs. 2–4 and Fig. 11 in Almers and McCleskey, 1984).

In all the models formulated in this paper, we have corrected for this limitation of Eyring theory in an approximate, but dimensionally correct fashion, sketched originally by Lauger (1973). The rate constants predicted by strict Eyring theory assume unity for the expectation value of the number of ions within jump distance of the transition barrier in question. With regard to the entry of a permeant ion into the channel, such an expectation value would not be unity, but rather a function of both permeant ion activity, and the geometry of the channel mouth. As a first-order of approximation, we have condensed the contribution of channel architecture into a single term, the capture radius of the channel, R_c. Any ion within a half-sphere defined by R_c, the "capture volume," is assumed to be within the jump distance of the entry barrier. Thus, in addition to the frequency factor Q (assumed $\sim kT/h$, in s^{-1}), the rate constants for entry into the channel are multiplied by an additional preexponential factor:

$$CRV = (N_A \times 2 \times \pi \times R_c^3/3), \tag{A-1}$$

where CRV (with units of M^{-1}) expresses the expected number of ions that would be found within the capture volume, given a bulk solution activity of 1 M, and N_A is Avogadro's num-

ber. Assuming a capture radius of 1.75 A (Lansman et al., 1986), the *CRV* is 6.76 × 10^{-3} M^{-1}. Thus, the rate of entry of extracellular Ba ions into an empty channel would be B_o × *CRV* × *Q* × exponential terms, where B_o is the extracellular Ba ion activity in molar and *CRV* × *Q* has units of $M^{-1}s^{-1}$.

Single-Site, Three-Ionic-Species Permeation Model

This section details the single binding site permeation model elaborated in Fig. 1 with entry and exit barrier heights and positions as described in the figure legend. Ion flux through a single-site channel in the presence of the permeant ions (K, Ba, and Ca) is determined by three sets of rate equations of the form:

$$O + X_o \underset{XM1}{\overset{X1}{\rightleftharpoons}} O - X \underset{XM2}{\overset{X2}{\rightleftharpoons}} O + X_i, \tag{A-2}$$

where X refers to K, Ba, or Ca (hereafter, abbreviated *K*, *B*, or *C* in rate constant and activity expressions), the subscripts "o" and "i" refer to extracellular and intracellular moieties, *O* represents an unoccupied channel, and the rate constants have their usual meanings. Taking into account that the probabilities of all channel states must sum to unity, one can derive the following expression for total ion flux through the single-site channel (outward current is positive):

$$I = PCQ\frac{\begin{array}{c}(Z_c F CM1)[CM2/(C2 + CM1)]C_i + (Z_B F BM1)[BM2/(B2 + BM1)]B_i \\ + (Z_K F KM2)[KM1/(K2 + KM1)]K_i - (Z_c F C1)[C2/(C2 + CM1)]C_o \\ - (Z_B F B1)[B2/(B2 + BM1)]B_o - (Z_K F K1)[K2/(K2 + KM1)]K_o\end{array}}{\begin{array}{c}1 + B_o[B1/(B2 + BM1)] + B_i[BM2/(B2 + BM1)] + C_o(C1/(C2 + CM1)] \\ + C_i[CM2/(C2 + CM1)] + K_o[K1/(K2 + KM1)] + K_i[KM2/(K2 + KM1)]\end{array}} \tag{A-3}$$

where *I* is in units of picoamperes; *PCQ* is 1.6 × 10^{-7} pC/elementary charge; and the rate constants follow standard Eyring theory as described by Hille and Schwarz (1978), with the addition of the capture volume modification described above for entry rates. Eq. A-3 was used to produce the current–voltage relations in Fig. 1.

Dual-Site, Three-Ionic-Species Permeation Model

This section details the dual binding-site permeation model elaborated in Fig. 9, with the heights and positions of the barriers and wells as described in the figure legend. The rate equations describing ion flux through the channel with three permeant ions (K, Ba, and Ca) are:

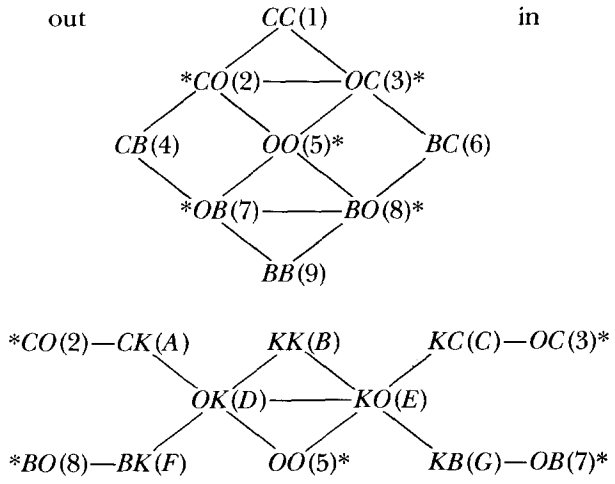

(A-4)

where *C, B,* and *K* refer to sites occupied by Ca, Ba, and K ions, respectively; *O* refers to an unoccupied site; the site closer to the outside appears on the left (e.g., *BO* refers to a channel with Ba in the site closest to the outside, the inner site being unoccupied), each state is given a shortened name in parentheses; and the upper and lower networks are connected at the states signified with an asterisk.

Rate constants mimic the situation for the single-site model above, except for the inclusion of electrical repulsion terms as formulated by Hille and Schwarz (1978). The system of differential equations describing Eq. A-4 results in a 16 × 16 matrix equation, and can be solved for the steady-state probabilities of the channel being in various states [$P(j)$] by numerical matrix inversion following the example of Begenisich and Cahalan (1980). Single-channel flux was calculated as $I_{ca}+I_{Ba}+I_K$ in picoamperes from the following expressions (outward current positive):

$$I_{Ca} = PCQ \times Z_C \times [P(7) \times CON78 - P(8) \times CON87]$$

$$I_{Ba} = PCQ \times Z_B \times [P(3) \times CON32 - P(2) \times CON23]$$

$$I_K = PCQ \times Z_K \times [P(D) \times CONDE - P(E) \times CONED]$$

where the rate constant *CONij* governs transitions from state *i* to *j*, and *Z* refers to valence of the corresponding cation. Slope conductances were calculated from the difference in fluxes for total or ion-specific current at −20 and −80 mV. The probabilities of single- and double-ion occupancy are obtained from $P(7)+P(8)$ and $P(9)$, respectively. The entire calculation was implemented in Lotus 1-2-3, using macro programs and the built-in matrix inversion function.

Triple-Site, Single-Species Permeation Model

This section details the triple binding-site permeation model elaborated in Fig. 11, with the heights and positions of the barriers and wells as described in the figure legend. The entry and exit peaks, wells, and intermediate barriers are arranged at electrical distances (*DIS*1, . . . , *DIS*7) of 0.01, 0.08, 0.321, 0.562, 0.6701, 0.779, and 0.822 of the way across the membrane field (outside to inside). *DIS*0 and *DIS*8 are defined as zero and unity, respectively. The rate equations describing ion flux through the channel with Ba as the only appreciably permeant ion are:

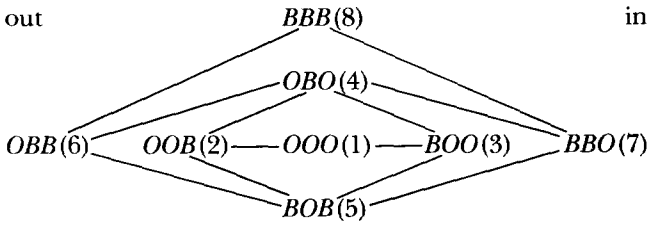

(A-5)

where *B* refers to sites occupied by a Ba ion; *O* refers to an unoccupied site; the site closer to the outside appears on the left (e.g., *BOO* refers to a channel with Ba in the site closest to the outside, the middle and inner sites being unoccupied); and each state is referred to by number as in the parentheses.

Rate constants follow the form of those described above for the dual-site model, except that the influence of electrostatic repulsion between ions had to be formulated in a more explicit manner to take into account the multitude of possible electrostatic interactions among three ions. Coulomb's law states that electrical repulsion energy between two ions

should be given by:

$$\ln (F_r)\, Z_i\, Z_j/(r_i - r_j)$$

where F_r is a repulsion factor (≥ 1) that takes into account the dielectric constant in the channel, Z refers to valence, r refers to distance of ions i and j to a common axial reference point. We assume that electrostatic repulsion within the pore is governed by the same electrical distances that describe the fall of transmembrane electric field (*DIS*1 . . . *DIS*7), and that, for simplicity, repulsive forces are not allowed to extend into the mouths of the channel. As examples, two of the repulsion interaction terms which contribute multiplicatively to the determination of various rate constants are given below. The first factor relates movement from the channel mouth into the pore; the second refers to movement within the channel permeation pathway:

$$FIN013 = (F_r)^{\{-[Z_R \times Z_R/(DIS6 - DIS1)]\}}$$
$$FIN123 = (F_r)^{\{-Z_R \times Z_R[1/(DIS6 - DIS3) - 1/(DIS6 - DIS2)]\}},$$

where, e.g., *FIN*123 attenuates rate constants describing the transition of a cation from site 1 to site 2 of the channel, given that another cation is already in site 3 (2 closer to 3 than to 1). Analogous *FOUTxyz* terms, with positive exponents, increase rate constants for transitions from site x to site y, given that an ion already resides at site z (this time, y further from z than x). The "site" numbers 0–4 correspond, respectively, to the extracellular space, the three wells (outside to inside), and the intracellular space. When two ions reside in the channel, the appropriate repulsion interaction terms can be multiplied together to produce the net effect of electrostatic interactions, since electrical potential energies are additive.

The system of differential equations corresponding to Eq. A-5 yields an 8 × 8 square matrix, the ij elements of which are composed of various combinations of the rate constants. Matrix inversion yields the steady-state probabilities of the channel being in various states. Single-channel flux was calculated in picoamperes as:

$$PCQ \times Z_R \times [P(2) \times CON24 - P(4) \times CON42 + P(5) \times CON57 - P(7) \times CON75]$$

where CONij are rate constants for transitions from states i to j. Slope conductances were calculated from the difference in flux at −20 and −80 mV. The probability of double- and triple-ion occupancy of the channel are calculated from $P(5) + P(6) + P(7)$ and $P(8)$, respectively. The entire calculation was implemented in Lotus 1-2-3.

We gratefully acknowledge John H. Lawrence for help with data analysis, and Stefan Herzig for comments on the manuscript.

This work was supported by National Institutes of Health grant RO1 HL-36957 to Eduardo Marban. David T. Yue is a Pfizer New Faculty Scholar and the Young Investigator of the American Heart Association, Maryland Affiliate. Eduardo Marban is the recipient of a Research Career Development Award from the National Institutes of Health (KO4 HL-01872).

Original version received 7 November 1988 and accepted version received 18 August 1989.

REFERENCES

Almers, W., and E. W. McCleskey. 1984. Non-selective conductance in calcium channels of frog muscle: calcium selectivity in a single-file pore. *Journal of Physiology.* 353:585–608.

Almers, W., E. W. McCleskey, and P. T. Palade. 1984. A non-selective cation conductance in frog muscle membrane blocked by micromolar external calcium ions. *Journal of Physiology.* 353:565–583.

Armstrong, C. M., and J. Lopez-Barneo. 1987. External calcium ions are required for potassium channel gating in squid neurons. *Science.* 236:712–714.

Begenisich, T. B., and M. D. Cahalan. 1980. Sodium channel permeation in squid axons. I. Reversal potential experiments. *Journal of Physiology.* 307:217–242.

Bell, C., and C. Miller. 1984. Effects of phospholipid surface charge on ion conductance in the K^+ channel of sarcoplasmic reticulum. *Biophysical Journal.* 45:279–287.

Blinks, J. R., W. G. Wier, P. Hess, and F. G. Prendergast. 1982. Measurement of Ca^{2+} concentrations in living cells. *Progress in Biophysics and Molecular Biology.* 40:1–114.

Byerly, L., P. B. Chase, and J. R. Stimers. 1985. Permeation and interaction of divalent cations in calcium channels of snail neurons. *Journal of General Physiology.* 85:491–518.

Campbell, D. L., W. R. Giles, J. R. Hume, D. Noble, and E. F. Shibata. 1988. Ion transfer characteristics of the calcium current in bull-frog atrial myocytes. *Journal of Physiology.* 403:239–266.

Campbell, D., R. L. Rasmussen, and H. C. Strauss. 1988. Theoretical study of the voltage and concentration dependence of the anomalous mole fraction effect in single calcium channels. *Biophysical Journal.* 54:945–954.

Cavalie, A., R. Ochi, D. Pelzer, and W. Trautwein. 1983. Elementary currents through Ca^{2+} channels in guinea pig myocytes. *Pflügers Archiv.* 398:284–297.

Cavalie, A., D. Pelzer, and W. Trautwein. 1986. Fast and slow gating behaviour of single calcium channels in cardiac cells: relation to activation and inactivation of calcium-channel current. *Pflügers Archiv.* 406:241–258.

Chesnoy-Marchais, D. 1985. Kinetic properties and selectivity of calcium-permeable single channels in *Aplysia* neurones. *Journal of Physiology.* 367:457–488.

Cooper, K. E., P. Y. Gates, and R. S. Eisenberg. 1988. Surmounting barriers in ionic channels. *Quarterly Reviews of Biophysics.* 21:331–364.

Coronado, R., and H. Affolter. 1986. Insulation of the conductance pathway of skeletal muscle transverse tubules from the surface charge of bilayer phospholipid. *Journal of General Physiology.* 87:933–953.

Cota, G., and C. M. Armstrong. 1988. Potassium channel "inactivation" induced by soft-glass patch pipettes. *Biophysical Journal.* 53:107–109.

Draper, N. R., and H. Smith. 1981. Applied Regression Analysis. 2nd edition. Wiley-Interscience, New York. 94, 462–468, 472.

Fenwick, E. M., A. Marty, and E. Neher. 1982. Sodium and calcium channels in bovine chromaffin cells. *Journal of Physiology.* 331:599–635.

Friel, D. D., and R. W. Tsien. 1989. Voltage-gated calcium channels: direct observation of the anomalous mole fraction effect at the single-channel level. *Proceedings of the National Academy of Sciences.* 86:5207–5211.

Furman, R. E., and J. C. Tanaka. 1988. Patch electrode glass composition affects ion channel currents. *Biophysical Journal.* 53:287–292.

Ganitkevitch, V. Y., M. F. Shuba, and S. V. Smirnov. 1988. Saturation of calcium channels in single isolated smooth muscle cells of guinea-pig taenia caeci. *Journal of Physiology.* 399:419–436.

Green, W. N., L. B. Weiss, and O. S. Andersen. 1987. Batrachotoxin-modified sodium channels in planar lipid bilayers. *Journal of General Physiology.* 89:841–872.

Hadley, R. W., and J. Hume. 1987. An intrinsic potential-dependent inactivation mechanism associated with calcium channels in guinea-pig ventricular myocytes. *Journal of Physiology.* 389:205–222.

Hamill, O. P., M. E. Neher, B. Sakmann, and F. J. Sigworth. 1981. Improved patch-clamp techniques for high-resolution current recording from cells and cell-free membrane patches. *Pflügers Archiv.* 391:85–100.

Harned, H. S., and B. B. Owen. 1958. The Physical Chemistry of Electrolyte Solutions. 3rd edition. Reinhold Publishing Corp., New York.

Hess, P., J. B. Lansman, and R. W. Tsien. 1984. Different modes of Ca channel gating behavior favoured by dihydropyridine agonists and antagonists. *Nature.* 311:538–544.

Hess, P., J. B. Lansman, and R. W. Tsien. 1986. Calcium channel selectivity for divalent and monovalent cations. *Journal of General Physiology.* 88:293–319.

Hess, P., and R. W. Tsien. 1984. Mechanism of ion permeation through calcium channels. *Nature.* 309:453–456.

Hille, B., and W. Schwarz. 1978. Potassium channels as multi-ion, single-file pores. *Journal of General Physiology.* 72:409–442.

Huang, Y., J. M. Quayle, J. F. Worley, N. B. Standen, and M. T. Nelson. 1989. External cadmium and internal cadmium block of single calcium channels in smooth muscle cells from rabbit mesenteric artery. *Biophysical Journal.* 56:1023–1028.

Kameyama, M., A. Kameyama, T. Nakayama, and M. Kaibara. 1988. Tissue extract recovers cardiac calcium channels from "run-down." *Pflügers Archiv.* 412:328–330.

Kostyuk, P. G., and S. L. Mironov. 1986. Some predictions concerning the calcium-channel model with different conformational states. *General Physiology and Biophysics.* 5:649–654.

Kostyuk, P. G., S. L. Mironov, and M. Shuba. 1983. Two ion-selecting filters in the calcium channel of the somatic membrane of mollusc neurons. *Journal of Membrane Biology.* 76:83–93.

Lansman, J. B., P. Hess, and R. W. Tsien. 1986. Blockade of current through single calcium channels by Cd^{2+}, Mg^{2+}, and Ca^{2+}. *Journal of General Physiology.* 88:321–347.

Lauger, P. 1973. Ion transport through pores: a rate-theory analysis. *Biochemica et Biophysica Acta.* 311:423–441.

Lee, K. S., E. Marban, and R. W. Tsien. 1985. Inactivation of calcium channels in mammalian heart cells: joint dependence on membrane potential and intracellular calcium. *Journal of Physiology.* 364:395–411.

Lee, K. S., and R. W. Tsien. 1984. High selectivity of calcium channels in single ventricular heart cells of the guinea pig. *Journal of Physiology.* 354:253–272.

Ma, J., and R. Coroado. 1987. Calcium channel conductance-activity curve in symmetrical barium solutions reveals multiple binding sites. *Biophysical Journal.* 51:423*a*. (Abstr.)

Ma, J., and R. Coronado. 1988. Conductance-activity, current-voltage, and mole fraction relationships for calcium channels. *Biophysical Journal.* 53:556*a*. (Abstr.)

Marban, E., and D. T. Yue. 1989. Ion permeation in L-type Ca channels: evidence for triple-ion occupany in the conduction pathway. *Biophysical Journal.* 55:594a. (Abstr.)

Marty, A. 1981. Ca-dependent K channels with large unitary conductance in chromaffin cell membranes. *Nature.* 291:497–500.

McDonald, T. F., A. Cavalie, W. Trautwein, and D. Pelzer. 1986. Voltage-dependent properties of macroscopic and elementary calcium channel currents in guinea pig ventricular myocytes. *Pflügers Archiv.* 406:437–448.

McLaughlin, S. 1977. Electrostatic potentials and membrane-solution interfaces. *Current Topics in Membrane Transport.* 9:71–144.

Mikami, A., K. Imoto, T. Tanabe, T. Niidome, Y. Mori, H. Takeshima, S. Narumiya, and S. Numa. 1989. Primary structure and functional expression of the cardiac dihydropyridine-sensitive calcium channel. *Nature.* 340:230–233.

Mitra, R., and M. Morad. 1986. Two types of calcium channels in guinea pig ventricular myocytes. *Proceedings of the National Academy of Sciences.* 83:5340–5344.

Neyton, J., and C. Miller. 1988. Discrete Ba^{2+} block as a probe of ion occupancy and pore structure in the high-conductance Ca^{2+}-activated K^+ channel. *Journal of General Physiology.* 92:569–586.

Nilius, B., P. Hess, J. B. Lansman, and R. W. Tsien. 1985. A novel type of cardiac calcium channel in ventricular cells. *Nature.* 316:443–446.

Pietrobon, D., B. Prod'hom, and P. Hess. 1988. Conformational changes associated with ion permeation in L-type calcium channels. *Nature.* 333:373–376.

Piskiewicz, D. 1977. Kinetics of Chemical and Enzyme-catalyzed Reactions. Oxford University Press, New York.

Prod'hom, B., D. Pietrobon, and P. Hess. 1987. Direct measurement of proton transfer rates to a group controlling the dihydropyridine-sensitive Ca^{2+} channel. *Nature.* 329:243–246.

Reuter, H., C. F. Stevens, R. W. Tsien, and G. Yellen. 1982. Properties of single calcium channels in cardiac cell culture. *Nature.* 297:501–504.

Rosenberg, R. L., P. Hess, J. P. Reeves, H. Smilowitz, and R. W. Tsien. 1986. Calcium channels in planar lipid bilayers: insights into mechanisms of ion permeation and gating. *Science.* 231:1564–1566.

Rosenberg, R. L., P. Hess, and R. W. Tsien. 1988. Cardiac calcium channels in planar lipid bilayers. *Journal of General Physiology.* 92:27–54.

Yatani, A., M. Goto, and Y. Tsuda. 1978. Nature of catecholamine-like actions of ATP and other energy-rich nucleotides on the bullfrog atrial muscle. *Japanese Journal of Physiology.* 28:47–61.

Yellen, G. 1982. Single Ca^{++}-activated nonselective cation channels in neuroblastoma. *Nature.* 296:357–359.

Yellen, G. 1984. Relief of Na^{+} block of Ca^{2+}-activated K^{+} channels by external cations. *Journal of General Physiology.* 84:187–199.

Yue, D. T., J. H. Lawrence, and E. Marban. 1989. Two molecular transitions influence cardiac sodium channel gating. *Science.* 244:349–352.

Yue, D. T., and E. Marban. 1987. Single Ca channel currents carried by Ca and Ba in heart cells: no anomalous mole fraction effect. *Circulation* 76 (Suppl. IV):IV-330 (Abstr.)

Yue, D. T., and E. Marban. 1988*a*. A novel cardiac potassium channel that is active and conductive at depolarized potentials. *Pflügers Archiv.* 413:127–133.

Yue, D. T., and E. Marban. 1988*b*. Ion movement in single Ca channels: novel evidence for multi-ion occupancy. *Circulation.* 78:II-409. (Abstr.)